Applied Catalysis B: Environmental 154–155 (2014) 62–72

Contents lists available at ScienceDirect

Applied Catalysis B: Environmental

journal homepage: www.elsevier.com/locate/apcatb

Kinetic evaluation of direct NO decomposition and NO–CO reaction over dendrimer-derived bimetallic Ir–Au/Al_2O_3 catalysts

You-Jung Song [a], Yaritza M. López-De Jesús [a,1], Paul T. Fanson [b], Christopher T. Williams [a,*]

[a] Department of Chemical Engineering, Swearingen Engineering Center, University of South Carolina, Columbia, SC 29208, USA
[b] Toyota Motor Engineering & Manufacturing North America, Inc, 1555 Woodridge Ave., Ann Arbor, MI 48105, USA

ARTICLE INFO

Article history:
Received 10 October 2013
Received in revised form
18 December 2013
Accepted 31 January 2014
Available online 9 February 2014

Keywords:
Iridium
Gold
Bimetallic
Dendrimer
Direct NO decomposition
NO–CO reaction

ABSTRACT

The effects of Au on the catalytic performance of Ir metal towards NO reduction by CO and direct NO decomposition have been investigated over dendrimer-derived Ir–Au bimetallic catalyst. Results were also compared to a catalyst prepared by conventional incipient wetness impregnation of metal salts. Characterization of Ir–Au bimetallic samples using scanning transmission electron microscopy, H_2 chemisorption and temperature programmed desorption of NO reveals that highly dispersed Ir–Au particles can be obtained by dendrimer templating method. In-situ transmission Fourier transform infrared spectroscopy following adsorption of probe molecules (i.e., CO and NO) on the dendrimer-derived Ir–Au bimetallic sample indicated the presence of electron transfer from Ir to Au sites. In contrast, a geometric effect of Au on Ir was observed over the conventional-derived sample, consistent with X-ray photoelectron spectroscopy measurements. These properties influence the catalytic performance, with higher selectivity towards N_2O and a better intrinsic catalytic turnover frequency for reduction of NO by CO and NO decomposition observed for the dendrimer-derived sample. Overall, the results suggest that both NO–CO and NO decomposition reaction are structure-sensitive reactions.

1. Introduction

The exhaust gases from automobile engines and industrial plants contain mainly oxides of carbon (CO and CO_2) and nitrogen (NO_x), hydrocarbons (HC), sulphur dioxide (SO_2), particulates and soot. One of the most urgent problems is removal of NO_x, typically produced during high-temperature combustion, which contributes to formation of smog and ground-level ozone by reacting with hydrocarbons in the presence of sunlight. More stringent NO_x emission requirements are being issued every day, necessitating development of more effective catalytic NO_x abatement technologies. Direct NO decomposition to N_2 and O_2 (without an added reductant) is an attractive alternative to NO_x traps and selective catalytic reduction for this application [1]. Thermodynamically, NO_x is unstable and tends to decompose through reactions such as

$$NO \leftrightarrow \frac{1}{2}N_2 + \frac{1}{2}O_2 \Delta G_f^0 = -86 \quad kJ \quad mol^{-1} \tag{1}$$

The equilibrium concentration of nitric oxide in the air is high at elevated temperatures (for example, 2×10^4 ppm at 2273 K), but decreases with the temperature (less than 200 ppm at $T < 1273$ K). Therefore, a direct decomposition reaction at moderate temperature should be an attractive method for NO_x abatement. However, the obstacle in using reaction (1) for the NO_x emission control involves finding a proper catalyst for decreasing its huge energy barrier ($E_a = 364$ kJ mol^{-1}) [2].

Supported Group VIII metals, such as Pt, Pd, Rh and Ir exhibit varying degrees of NO decomposition activity, albeit at high temperatures (600–800 °C) [3–5]. Supported Pt and Pd exhibited good initial decomposition activity; however, they deactivate rapidly at low temperatures due to oxygen poisoning [3,6]. Ir, on the other hand, exhibits superior ability to convert NO under oxidizing conditions. Tauster and Murrell [7] were the first who studied NO reduction by CO with Ir catalysts. They showed that Ir is the only noble metal favoring the NO–CO over the CO–O_2 reaction in the presence of O_2. Absorbed oxygen on Ir was the predominant surface species and its reaction with gaseous CO generated free surface sites. These sites were available for the chemisorption of NO and O_2. Taylor and Schlatter [8], who studied NO reduction by CO in the presence of O_2 over alumina-supported Ir, Rh, Pt and Pd catalysts, confirmed these results. The high effectiveness of Ir compared to the other metals was attributed to its ability to adsorb NO dissociatively in the presence of excess O_2.

* Corresponding author. Tel.: +1 803 777 0143; fax: +1 803 777 8265.
E-mail address: willia84@cec.sc.edu (C.T. Williams).
[1] Current address: Johnson Matthey, Emission Control Technologies, 900 Forge Avenue, Suite 100, Audubon, PA 19403-2305, USA.

http://dx.doi.org/10.1016/j.apcatb.2014.01.065
0926-3373/

Recently, an increasing number of studies have shown the advantage of the use of bimetallic clusters, which often provide enhanced selectivity, stability, and/or activity, in catalysis [9–14]. Among them, Peng et al. and Wang et al. reported the benefit of the addition of other elements to the Pd active site through the formation of bimetallic clusters in the activity of CO oxidation [13,14]. They especially focused on Au [13] and Ag [14] as additives, since these are elements with high resistance to oxidation might keep nearby Pd metal atoms in their metallic state. Here, the combination of Au or Ag with Ir would also be beneficial and therefore Au was selected as an additive and Ir–Au bimetallic clusters were examined for NO decomposition.

Different Ir-based catalysts have been recently prepared and tested [15–24], with most studies revealing that the effect of the size of Ir particles on the deNO_x activity was crucial [20–24] and related [7,8,25] to the competitive reactions of CO with NO and CO with O_2. Activation of the Ir catalysts was achieved by high temperature pretreatments [17,18,26] or by in situ activation during catalytic tests [20,21]. Both methods led to crystallite growth and a coexistence of Ir and IrO_2 [20,23]. Thus, size control of Ir-based catalysts is needed to achieve optimal performance for the simultaneous reduction of NO and CO emissions.

In order to obtain size-controlled uniform materials, several synthetic techniques have been developed over the years including the use of polymers, surfactants, well-defined organometallic cluster complexes, size-selected metal clusters and ionic liquids. One recent method that has received considerable attention is the use of dendrimer–metal nanocomposites (DMNs) as precursors [27]. Dendrimers [28,29] are monodisperse, hyperbranched spherical polymers that emanate from a central core with repetitive branching units, allowing for controllable size. While possessing a very dense exterior, they contain less dense interiors that can be ideal for encapsulation of metal nanoparticles. The use of dendrimers as templates/stabilizers for synthesis of nanoparticles is a relatively new but active field. There are now many investigations exploring the use of DMNs as precursors to synthesize supported catalysts, and narrow metal particle size distributions have been observed for different transition metals such as Pt, Pd, Au, Ru, Cu, Pt-Pd, Pt-Au, Pd-Au, and Ag–Au catalysts (see for example [30–38]. Most recently, we found that dendrimer-derived Ir–Au bimetallic catalyst with higher dispersion compared to conventionally derived catalyst resulted in an enhanced activity for the CO oxidation reaction [39].

The scope of the present work is to characterize a series of Ir–Au catalysts in order to derive relations between physicochemical and catalytic properties for NO reduction and CO oxidation and for direct NO decomposition. It was found that dendrimer-derived bimetallic catalyst (Ir–Au-DD) exhibited highly dispersed metal nanoparticles and narrow size distribution when compared with conventionally prepared sample (Ir–Au-CD). However, Ir–Au-DD showed similar activity for the NO–CO and direct NO decomposition reactions compared with Ir monometallic catalyst, whereas an enhanced activity was found on Ir–Au-CD.

2. Materials and methods

2.1. Materials

Fourth generation hydroxyl-terminated poly(amido)amine (PAMAM) dendrimer (G4OH) (10 wt% in methanol solution) was obtained from Aldrich. Prior to use, an aqueous solution was made by evaporating methanol with flowing N_2 and diluting the residue to 1.7×10^{-4} M with deionized water. $IrCl_3{\cdot}3H_2O$ (AlfaAesar), $HAuCl_4$ (Aldrich) and $NaBH_4$ (granules, 99.995%, Aldrich) were used as received. Deionized water (18 MΩ cm Milli-Q) was used to prepare all the aqueous solutions. A gamma-delta-theta phase alumina (specific surface area = 104 $m^2\,g^{-1}$, pore volume = 0.9 $mL\,g^{-1}$) was provided by Toyota. NO, CO, O_2 (UHP), He (UHP) and H_2 (UHP) were supplied by Airstar.

2.2. Catalyst preparation

The synthesis of dendrimer–metal nanocomposites was adapted from the literature [40–43] and has been published previously [44]. A proper amount of 8.0×10^{-3} M $IrCl_3{\cdot}3H_2O$ precursor solution was added under N_2 purging to G4OH dendrimer solution with the concentration of 1.7×10^{-4} M to reach a molar ratio of Ir^{3+} to G4OH of 20:1. The mixed solution was stirred for 7 days at room temperature with N_2 flowing to protect the Ir^{3+} ions from oxidation by dissolved O_2 and allow the complexation of Ir^{3+} ions with the functional groups in G4OH dendrimer. The formation of dendrimer encapsulated metallic Ir nanoparticles in solution was attempted by adding a 10-fold excess solution of $NaBH_4$ at room temperature. The supported catalyst was made by standard wet impregnation of the reduced dendrimer-Ir nanocomposite onto Al_2O_3, to a nominal Ir loading of 1.0 wt % (Ir-DD). The extra water was removed under ambient conditions by evaporation of the stirring slurry for 3 days. The same procedure was used to make dendrimer-Au monometallic nanocomposites except allowing complexation time of 2 min, with the corresponding supported catalyst having a nominal Au loading of 1.0 wt% (Au-DD).

The sequential method was followed for bimetallic Ir–Au DMNs, which involved first mixing Ir metal precursor solution with dendrimer solution for 7 days under N_2 purging. Then, Au metal precursor solution was added, whereupon complexation occurred (for a short period, order of minutes). In this case, the target ratio of each type of metal atom to dendrimer was 20 to 1, thus making a total metal atom loading of 40 atoms per dendrimer. Finally, these bimetal-dendrimer complex nanocomposites were impregnated onto alumina as described above, with the nominal loading of 1.0 wt% Ir and 1.0 wt% Au (Ir–Au-DD). For monometallic Ir and Au, and for Ir–Au DMN precursors, it is expected that the metal salts are fully complexed within the dendrimer interior based on previous studies of Ir [40,41] and Au (e.g., [42,43]) complexation using UV–visible spectroscopy [40,43] and EXAFS [41].

Conventional Ir and Au catalysts were made by incipient wetness method (Ir-CD and Au-CD). A proper amount of 5.78×10^{-2} M of $IrCl_3{\cdot}3H_2O$ precursor solution was added dropwise to Al_2O_3 and the resulting slurry was dried in an oven at 80 °C for overnight before use. A conventional Au catalyst was made with exactly the same protocol. In the case of conventional Ir–Au bimetallic catalyst (Ir–Au-CD), equal volumes of 11.56×10^{-2} M of $IrCl_3{\cdot}3H_2O$ and $HAuCl_4$ precursor solutions were mixed together and then added to the Al_2O_3. The nominal metal loadings of all the conventional catalysts were the same as their DMN-derived analogues.

All catalysts studied were activated under flowing O_2 treatment at 350 °C for 30 min and H_2 treatment at 400 °C for 1 h with a slow temperature ramp rate of 5 °C min^{-1} followed by cooling to room temperature. This activation protocol was adapted for consistency from a previous study [44] which showed that G4OH dendrimer template could be sufficiently decomposed on an γ-Al_2O_3 support to expose the metal nanoparticles.

2.3. Catalyst characterization

Scanning transmission electron microscopy (STEM) was conducted using a JEOL 2100F 200 kV FEG-STEM/TEM equipped with a CEOS Cs corrector system. High angle annular dark-field (HAADF) STEM images were acquired on a Fischione Model 3000 HAADF detector with a camera length such that the inner cut-off angle of the detector was 50 mrad. Holey-molybdenum coated Cu grids

were dipped into finely powdered catalysts samples for examination under the microscope. Histograms of particle size distribution were obtained by measuring at least 300 randomly selected particles from at least 6 different micrographs for any sample analyzed.

X-ray photoelectron spectroscopy measurements were made on selected samples using a Kratos AXIS Ultra DLD XPS system with a monochromatic Al *K*α source operated at 15 keV and 150 W and a hemispherical energy analyzer. All oxidized samples were reduced at 400 °C, the same temperature used for all other characterization methods, for experimental consistency. After pretreatment, the samples were transferred into the UHV chamber for XPS analysis without exposure to air. The XPS spectra were fitted to a Shirley-Linear background using XPSPEAK software version 4.1. The deconvolution was accomplished with Gaussian–Lorentzian band shapes. Appropriate peak positions, FWHM's and area constraints were used for peak splitting of 4f electron. The FWHM was maintained constant at ~2.0 eV for Ir 4f and ~1.3 eV for Au 4f electrons. The shifts reported are accurate to within ±0.1 eV. The Al(2p) binding energy (BE) was used as a reference and was compared to the literature value of 74.4 eV. The same difference (charging correction) in eV was applied to all other XPS peaks to give corrected BE's of Ir(4f), Au(4f) and O(1s) electrons for both monometallic and bimetallic systems.

Atomic absorption spectroscopy was performed on a Perkin-Elmer 3300 and used to determine the elemental concentrations of Ir and Au. The weight percentages of metals in the final bimetallic catalysts were determined by digesting 0.1 g of sample in aqua regia at 120 °C for 4 h and then diluting (~20 times) with DI water before analysis. A set of standards (known concentration of each specific element) was prepared to calibrate the instrument before the actual measurements were made.

Hydrogen chemisorption measurements were performed on an automated AutoChem II 2920 from Micromeritics. Approximately 0.1 g oxidized sample (350 °C for 30 min) was reduced *in-situ* in flowing H_2 (50 mL min^{-1}) at 400 °C for 1 h followed by Ar (50 mL min^{-1}) purging at the same temperature for 1 h to remove any residual H_2. The chemisorption experiments were done using the pulse methodology by dosing a known volume of 10% H_2/Ar in 4 min intervals. Chemisorbed hydrogen on the samples was measured at 40 °C and atmospheric pressure and the metallic dispersion and particle size were determined.

In situ FTIR spectra were recorded using a Nicolet Nexus 470 spectrometer equipped with mercury–cadmium–telluride B (MCT-B) detector cooled by liquid nitrogen. FTIR spectra were collected in single beam absorbance mode with a resolution of 4 cm^{-1} at room temperature. Catalysts samples of approximately 30 mg were prepared as self-supporting pellets with a diameter of 12 mm. All experiments were conducted in an externally-heated cylindrical sample cell as described previously [39]. Briefly, a total gas flow of ~70 mL min^{-1} entered the cell in front of the pellet and exited behind the pellet. The samples were reduced in H_2 for 1 h at 400 °C, cooled to RT in He, exposed to 1% CO in He until surface saturation, and then flushed with pure He to remove weakly bonded CO species and gas phase CO. The same procedure was used for adsorption of NO, except flowing 1% NO in He instead of CO gas mixture. All spectra were referenced to an initial background spectrum taken in He prior to CO or NO exposure. The curve fitting of these FTIR spectra was conducted with different fitting models (e.g., Gaussian, Lorentzian, log-normal) to obtain the peak position, width, height, and area of the overlapping peaks. Initially, the individual peak parameters (i.e. position, full width at half maximum (FWHM), and height) were chosen based on visual inspection of the experimental spectrum for the Ir-CD sample. Then, the residual between the overall fit and raw spectrum was minimized by minimizing the square root of the sum of square errors in an iterative fashion. The peak deconvolution using spectral curve fitting was continued for other samples in the similar fashion. It was found that all the peaks were effectively modeled by Gaussian line shapes.

2.4. Catalytic evaluation: NO–CO reaction and direct NO decomposition

The catalytic evaluation for the NO–CO and direct NO decomposition reactions were performed in a fixed-bed quartz reactor at atmospheric pressure using space velocities of 100,000 and 5000 mL g^{-1} h^{-1}, respectively. The temperature range was 25–600 °C with a ramp of 5 °C min^{-1}. For the NO–CO reaction, 60 mg of sample was loaded and the reaction feed contained 2000 ppm of NO and 2000 ppm of CO balanced with He. Direct NO decomposition was carried out with 200 mg of sample and the feed contained 2000 ppm of NO balanced with He. For temperature-programmed desorption of NO (NO-TPD), 50 sccm of 1% NO/He was used at room temperature for 30 min, followed by He purge for another 30 min, and then NO-TPD was recorded in He gas. The outlet of the reactor was monitored by means of a quadrupole mass spectrometer (MS) equipped with a fast response inlet capillary/leak valve system. All lines between the outlet of reactor and the inlet capillary of the MS, including also the latter, were held at 120 °C. Prior to the catalytic measurements, the oxidized samples were reduced in situ in flowing H_2 at 400 °C for 1 h. A flow of He gas was used for 30 min at the same temperature to purge the residual H_2 from the system, followed by system cooling to room temperature. Steady state for the reaction was considered achieved for a given temperature when the mass intensities for reactant and product species were constant with time. Mass numbers (*m/z*) of 2, 15, 18, 28, 30, 32, 44 and 46 represents H_2, NO, H_2O, N_2(CO), NO(NO_2), O_2, N_2O(CO_2) and NO_2, respectively.

For the calculation of turnover frequencies (TOFs) for the reactions over each catalyst, reaction rates calculated from the light-off curves at differential conversions (i.e., less than 20%) and metal dispersion derived from chemisorption data were used.

3. Results and discussion

3.1. Particle size, distribution and composition

The average particle sizes and metallic dispersions were determined by electron microscopy and H_2-chemisorption after activation using both treatment protocols (Table 1). STEM analysis and H_2-chemisorption data for alumina supported monometallic Ir and Au were reported before [39]. The Au monometallic catalysts exhibit a volume-to-surface mean diameter (VSMD) [45] that is much larger than the Ir monometallic catalysts (Table 1). The difference in average particle size between Ir and Au suggests that the latter has higher mobility on the alumina support than the former at the elevated oxidation and reduction temperatures used here. This in turn leads to more extensive sintering of Au nanoparticles. On the other hand, Ir–Au-CD and Ir–Au-DD bimetallic catalysts have smaller VSMDs than the Au monometallic catalysts (i.e., below 4 nm). Thus, it appears that the presence of Ir at these ratios prevents the sintering or agglomeration of Au. Atomic absorption spectroscopy analysis shows that there is no significant different between these two bimetallic catalysts in terms of the actual metal weight loading on alumina support. The loadings are similar to the nominal values and expected Ir to Au ratio (within the error of the measurement).

However, it was noticed that the morphology of these two bimetallic catalysts varies with different methods as shown in Fig. 1A and B. The conventional catalyst (Ir–Au-CD) has an asymmetric distribution with most (91%) of the particles between 0.5 and 2 nm and the remaining 9% of particles spread out between 2

Table 1
Metal particle size measured by STEM, dispersion by H_2 chemisorption, actual metal loading and bulk composition.

Catalysts	Mean diameter (nm)	Volume-to-surface mean diameter[a] (nm)	Dispersion[b] (%)	Metal weight loading[c]		Bulk composition[c]	
				Ir (%)	Au(%)	Ir (%)	Au(%)
Ir-CD	1.0 ± 0.2	1.1 ± 0.1	74 ± 7	1.0	–	100	–
Ir-DD	2.0 ± 0.4	2.1 ± 0.1	65 ± 9	1.0	–	100	–
Ir–Au-CD	1.5 ± 2.4	3.1 ± 0.8	10 ± 1	0.9	1.0	48	52
Ir–Au-DD	1.5 ± 0.3	1.6 ± 0.1	43 ± 3	1.0	1.0	50	50
Au-CD	4.9 ± 7.6	18.5 ± 1.6	–	–	0.9	–	100
Au-DD	9.6 ± 3.4	9.8 ± 0.9	–	–	0.7	–	100

[a] Calculated using $\bar{D} = \sum_i^N N_i D_{p,i}^3 / \sum_i^N N_i D_{p,i}^2$, where N_i is number of particles and $D_{p,i}$ is the measured diameter from STEM images [45].
[b] Obtained by H_2 chemisorption analysis. (H per Ir metal).
[c] Obtained by elemental analysis.

and 6 nm creating a broad particle size distribution. In contrast, in the Ir–Au-DD catalyst, very narrow particle size distribution with a more symmetric distribution was observed and no particles larger than 3 nm were observed. It is apparent that the conventional Ir–Au catalyst has a larger volume-surface mean diameter (3.1 ± 0.8 nm) with lower dispersion (10%) and broader size distribution than the dendrimer-derived Ir–Au catalysts with VSMD of 1.6 ± 0.1 nm and 43% dispersion, as listed in Table 1. This implies that G4OH PAMAM dendrimer exerts control over particle formation.

Although there is relatively little effect on controlling particle sizes when dendrimer precursors are used to prepare 1.0 wt% Ir monometallic catalyst, DMN precursors do appear to play a role in controlling the sintering/agglomeration processes of Ir–Au bimetallic and Au monometallic nanoparticles over alumina, thus influencing particle size and size distribution. This has been observed previously for other metals such as ruthenium and rhodium [41,42,46].

Fig. 2 shows the Ir 4f and Au 4f regions of the Ir–Au bimetallic samples that were investigated before and after NO decomposition reaction by XPS. All the spent bimetallic samples for NO decomposition reaction were re-reduced at 400 °C in the XPS main chamber for in situ sample pretreatment. The theoretical separations of the spin-orbit split components were 3.0 eV for Ir 4f and 3.7 eV for Au 4f. The full width at half maximum (FWHM) values of the 4f 7/2 and 4f 5/2 peaks were assumed to be identical. These fitting parameters were used in all the cases below for the metal peaks in spectra containing metal and/or oxide.

In Fig. 2A, the dendrimer-derived sample shows a broader band envelope compared to the conventional-derived sample, with four peaks at binding energies of 61, 62, 64 and 65 eV. The broader envelope corresponds to the relatively higher binding energies of 62 and 65 eV, which are associated with IrO_2. This suggests that it is harder for the dendrimer-derived sample to be reduced than for the conventionally derived sample under the same pretreatment

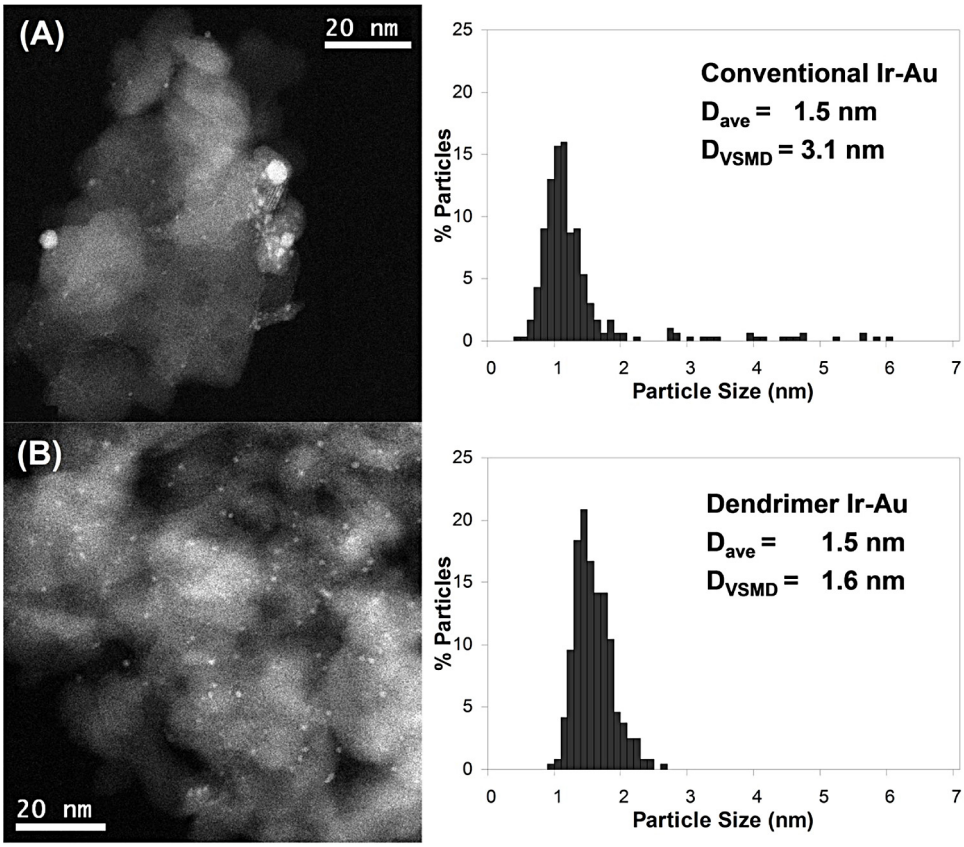

Fig. 1. STEM images and size distributions for (A) Ir–Au-CD and (B) Ir–Au-DD.

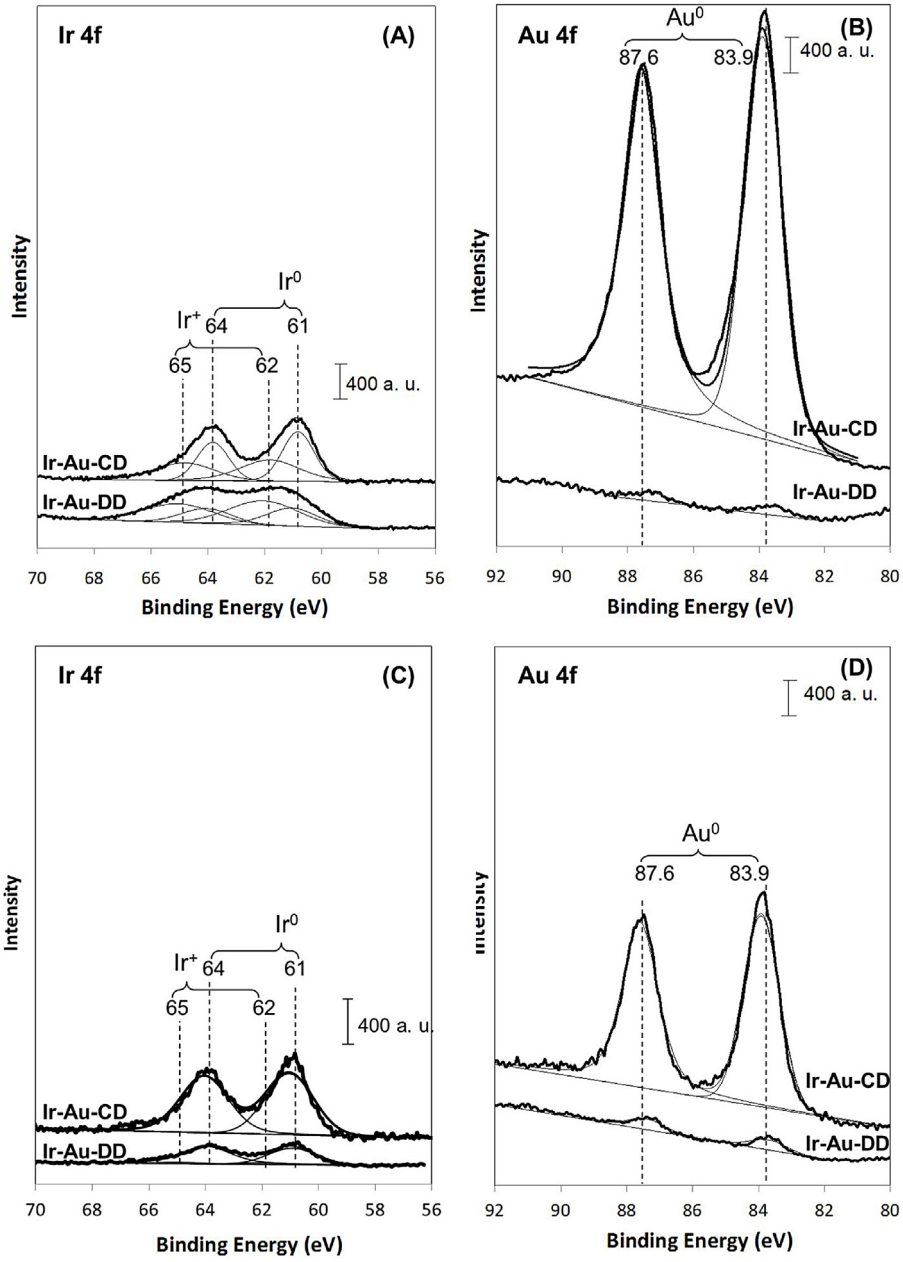

Fig. 2. XPS data for oxidation state of Ir and Au on Ir–Au-CD and Ir–Au-DD before (A and B) and after (C and D) NO decomposition reaction.

protocol. These oxidation peaks were gone for the spent catalysts of NO decomposition reaction after re-reduction step as shown in Fig. 2C. More interestingly, the Au 4f region for the conventional-derived sample shows greatly increased signal compared with Ir 4f signal, while the Au 4f signal of Ir–Au-DD is similar to or a little smaller than Ir 4f in terms of their intensities. This implies that these two samples that were synthesized different ways have different surface composition even though the bulk composition are similar each other based on the AA analysis. This might indicate that in the case of Ir–Au-CD, the Au is enriched on the surface by agglomeration of Au over Ir. Such an agglomeration of Au also affects the dispersion of Ir–Au-CD sample and leads to much lower dispersion when compared to Ir-CD (Table 1). Thus, the number of Ir active sites of the surface was significantly decreased by the presence of Au metal atoms. On the other hand, for Ir–Au-DD, it seems to have relatively well mixed surface of Ir and Au. Thus, this difference would be expected to affect the performance of the catalyst in the reactions.

3.2. Infrared spectra of adsorbed NO and CO

Infrared spectra collected following the adsorption of NO and CO at room temperature on the Ir monometallic and the Ir–Au bimetallic samples are shown in Fig. 3. In our previous work, we found that there are no characteristic ν_{NO} vibrations or ν_{CO} vibrations in the spectra of the Au-CD and Au-DD samples, which had an average Au particle size of approximately 19 and 10 nm (Table 1) [39]. This result is consistent with previous literature reports demonstrating that the adsorption of CO on Au depends on the particle size of the Au crystallites and is observed only on Au nanoparticles with sizes below 5 nm [47–49].

When the conventional and dendrimer-derived Ir monometallic samples were exposed to NO under similar conditions (Fig. 3A), three strong bands were observed at 1829, 1887 and 1956 cm^{-1} which can be assigned as linearly adsorbed NO on fully reduced Ir sites or on oxidized Ir sites, as listed in Table 2 [21,50,51]. In the same way, three strong bands were observed at 2008, 2040 and

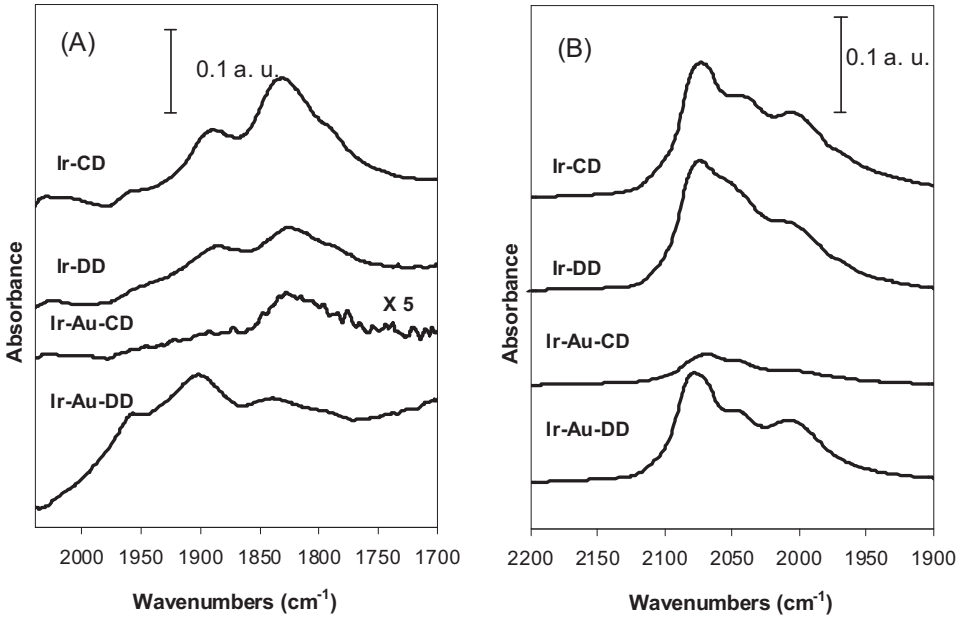

Fig. 3. FTIR results for (A) NO adsorption and (B) CO adsorption on Ir monometallic and Ir–Au bimetallic catalysts.

2074 cm^{-1} for the CO adsorption on two Ir monometallic samples (Fig. 3B). However, there are several peaks involved between 2000 and 2100 cm^{-1} and can generally be assigned to linearly adsorbed CO species on fully reduced Ir sites (2035, 2053 cm^{-1}) or on partially oxidized Ir sites (2092 cm^{-1}) or antisymmetric (2012 cm^{-1}) or symmetric (2078 cm^{-1}) vibrations of adsorbed dicarbonyl species on Ir ions (see Fig. S1 in Supporting information for detail). The assignment of these peaks in this small region is based on our previous published work [40] and the available literature [50,52–60].

In order to investigate the effect of Au on both conventional and dendrimer-derived bimetallic samples, the same FTIR experiment was carried out and the results are listed in Table 2 after the curve fitting. For the conventional bimetallic sample, it was clearly noticed that the intensity of spectra for both NO and CO adsorption were considerably depressed compared to the Ir monometallic sample. Also, a comparison of the spectrum characterizing the Ir–Au-CD sample with the one obtained for Ir-CD indicates that in this case the ν_{NO} and ν_{CO} bands were shifted to the lower wavenumbers by 7–8 cm^{-1}. Such a shift could be related to a variety of different reasons. The dispersion of metal for example, can play a role as it was observed earlier [54–56]. Indeed, the STEM data show that after oxidation/reduction treatment the Ir–Au-CD sample had a larger average metal particle size when compared to Ir-CD (Table 1). However, in this case, a blue shift in the ν_{CO} would be expected due to the increased coordination number of the surface Ir atoms in large particles, leading to the reduction of back-donation of electrons into the antibonding molecular orbitals of CO [57], which contradicts our observations. Another possible explanation could be related to a geometric effect, caused by a dilution of Ir surface sites by Au. If such dilution was to take place, the decreased dipole–dipole coupling between adsorbed CO molecules would result in a red shift in the ν_{CO}, consistent with our observations as well as the decreased peak intensities. The general behavior of NO during the adsorption on metal surfaces and the formation of M–NO bonds can be interpreted using the same arguments as proposed for the adsorption of CO [61]. This is because the similar distribution of electrons in CO and NO allows the use of both molecules to probe metal surfaces. Moreover, because NO has an extra electron occupying the π^* antibonding molecular orbital, it can be more sensitive to the electronic state of the adsorbate; in this orbital, even slight changes in the electron density noticeably change the frequency of the ν_{NO} vibrations [61]. The dilution of Ir surface sites by Au in the Ir–Au-CD sample can also explain the surface enrichment of Au that was observed in the XPS analysis.

When similar FTIR experiments were repeated with the dendrimer-derived bimetallic samples, on the other hand, there were no significant changes in the band strength in the spectra of NO and CO adsorption compared to the monometallic sample. These peak intensities could be related to Ir active sites exposed to the surface, indicating that Ir active sites on the surface of the Ir–Au-DD sample are not significantly decreased by the presence of Au metal atoms. This is consistent with our XPS result for the Ir and Au surface analysis. However, in the presence of Au in the bimetallic sample, the peak positions were different from the monometallic sample, with blue shifts in the ν_{NO} and ν_{CO} bands listed in Table 2. Since it was confirmed that the Ir–Au-DD sample had a smaller particle size than Ir-DD sample by STEM data, the dispersion of the metal is not the reason for the peak shift. Thus, the possible explanation for the shift could be an electronic effect caused by net electron transfer from Ir to Au. For example, such a transfer would result in a decrease in back-donation of electrons into the antibonding molecular orbitals of CO, resulting in a blue shift in

Table 2
NO and CO adsorption wavenumber (cm^{-1}) of all catalysts.

Catalysts	Linearly adsorbed NO		Linearly adsorbed CO		
	Ir^0–NO	Ir^+–NO	Ir^0–CO	Ir^+–CO	
Conventional-Derived	Ir-CD	1829, 1887	1956	2035, 2053	2092
	Ir–Au-CD	1821, 1880	1949	2027, 2046	2083
Dendrimer-derived	Ir-DD	1828, 1885	1954	2034, 2054	2093
	Ir–Au-DD	1844, 1899	1963	2041, 2063	2098

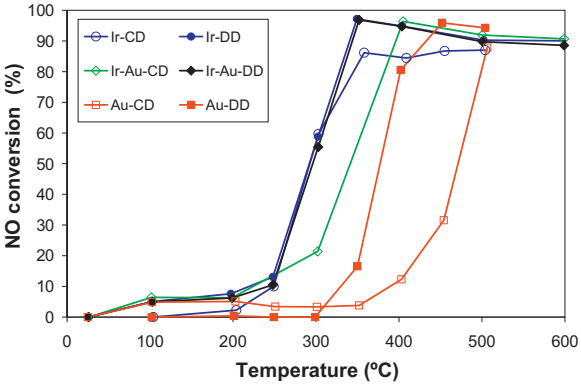

Fig. 4. NO–CO light-off curves for CD and DD catalysts.

ν_{CO}. Also, the position of ν_{NO} band shifted to higher wavenumbers in the Ir–Au-DD sample, similar to what was observed during the adsorption of CO on the same sample. This once again suggests that the electronic property of Ir was significantly affected by Au in the bimetallic sample.

3.3. Catalytic reduction of NO with CO

In order to evaluate catalytic activity of the catalysts, the NO–CO reaction was tested. As a result, light-off curves showing the temperature dependence of NO conversion for the NO–CO reaction over conventional and dendrimer-derived Al_2O_3-supported Ir–Au catalysts are shown in Fig. 4. As references, Ir and Au monometallic catalysts were also investigated. Since the CO is not labeled with ^{13}C isotope, we could not differentiate the N_2 formed and the CO consumed simultaneously, owing to the same mass numbers of N_2 and CO ($m/e = 28$). The same situation exists for CO_2 and N_2O ($m/e = 44$) and for NO and NO_2 ($m/e = 30$). In spite of this, we can still compare the de-NO_x activity of the Ir–Au bimetallic with that of Ir or Au monometallic catalysts from the decrease in NO concentration by following $m/e = 15$. In general, similar NO conversion behaviors were observed with conventional Ir and dendrimer-derived Ir catalysts, except that Ir-DD showed slightly higher NO conversion than Ir-CD above 350 °C. This indicates that the dendrimer templating approach does not play a significant role in this case. These catalytic performances were much better than that achieved over Au monometallic catalysts according to the higher NO conversion at the same reaction temperature for this NO–CO reaction (e.g., about 60% for Ir and below 5% for Au monometallic samples at around 300 °C). However, they cannot be simply compared to each other because the catalytic activity is dependent on various factors such as nature of the material and support, kind of precursors or size of metal, etc. Thus, it should be noted that Au monometalic samples have much larger particle size than the Ir monometallic samples, and such a poor control of the particle size may have led to low activity for the NO–CO reaction.

It has been reported that use of a secondary metal such as Au and Ag enhances activity for nitric oxide decomposition over supported Pt-group metals [62]. Furthermore, Qun and co-workers have demonstrated that Ir-based bifunctional catalyst can not only improve the catalytic performance but also enhance the stability under the strict conditions for direct and NO-assisted N_2O decomposition [63]. However, unlike our expectations, none of the bimetallic catalyst prepared in our work showed enhanced performance compared with the Ir monometallic catalyst. That is, almost the same catalytic performance was obtained on Ir-Au-DD as for Ir-DD, while the Ir–Au-CD showed even lower NO conversion than Ir-CD catalyst at the same reaction temperature (i.e., about 60% and

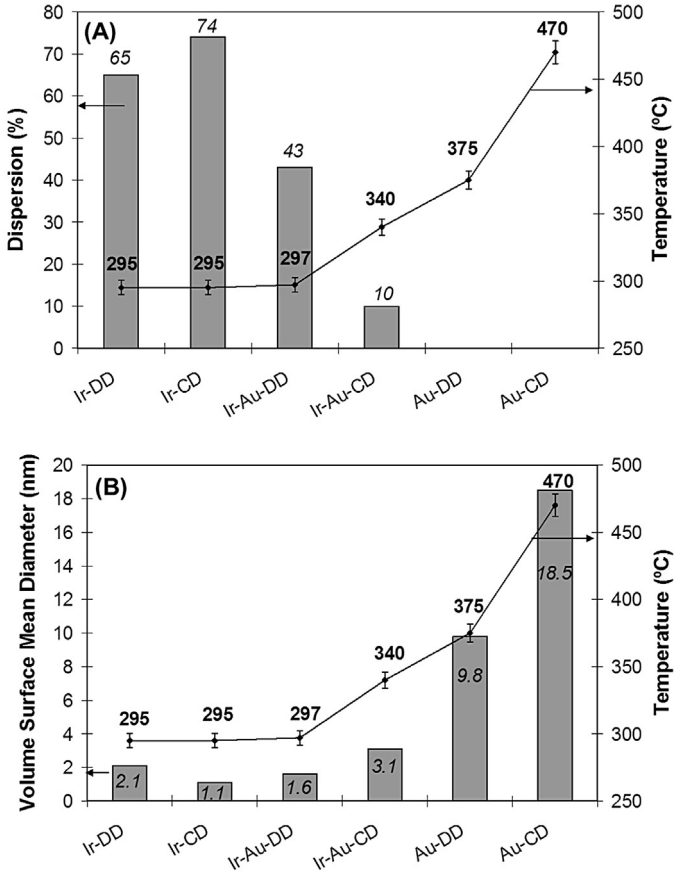

Fig. 5. Effect of dispersion and particle size of different catalysts on T_{50}.

20% for Ir–Au-DD and Ir–Au-CD sample, respectively, at around 300 °C). On the other hand, the dendrimer-derived samples such as Ir–Au-DD or Au-DD showed better catalytic activity than conventional Ir-Au-CD or Au-CD samples, respectively. This indicates that the dendrimer approach is an effective way to control Au metal size of the catalyst and can result in the improvement in catalytic performance. Such a conclusion is consistent with the STEM data as well as metal dispersion data presented above (see Fig. 1 and Table 1).

Fig. 5 reveals the relationship between dispersion and average particle size of the catalysts, and catalytic activity for NO–CO reaction, represented as T_{50} (i.e., temperature at 50% NO conversion) from the NO–CO light off curves. Previously, Davis and co-workers [64] have investigated the correlation between the Pd particle size and the catalytic activity toward the NO–CO reaction. In their work, it was found that Pd particles of 1 nm average diameter were more active for the NO–CO reaction than 4.5 nm Pd particles. In our work, although we are considering not just monometallic but bimetallic samples as well, it also seems that the catalysts with higher dispersion or with smaller particle size showed lower T_{50} values for the NO–CO reaction, as shown in Fig. 5A and B.

3.4. Catalytic direct NO decomposition

Fig. 6 shows light-off curves for direct NO decomposition with low gas hour space velocity of 5000 h^{-1} over conventional and dendrimer-derived Al_2O_3-supported Ir–Au bimetallic catalysts, Ir and Au monometallic catalysts and Al_2O_3 support. All the NO conversions under these reaction conditions were lower than 30% up to 500 °C. The general activity trend was similar to that obtained for the NO–CO reaction. That is, Ir monometallic catalysts showed

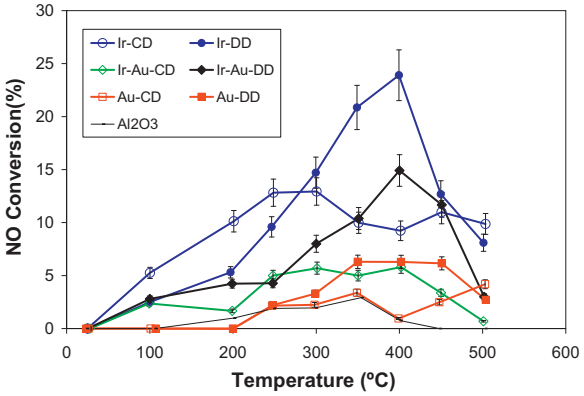

Fig. 6. NO decomposition light-off curves for CD and DD catalysts.

the best catalytic activity over almost the entire reaction temperature range. Conventional and dendrimer-derived Ir–Au bimetallic catalysts followed, and then very low activities (i.e., below 5% of NO conversion) were achieved over Au monometallic catalysts. Such a low NO conversion obtained on Au monometallic catalyst was almost the same as activity over support by itself, indicating that Au metal atoms were inactive for direct NO decomposition. The light-off curves characterizing both the conventional and dendrimer-derived Ir–Au catalysts were slightly better than that of Au monometallic and worse than that of Ir monometallic sample. This also indicates that the presence of Au in this sample has no substantial effect on Ir activity; Au rather remains as an inactive material.

In order to make clear the relationship between the catalytic performance and the adsorption behaviors of the Ir–Au bimetallic catalysts, we carried out TPD of NO over the bimetallic samples, and then made comparison with the TPD results over the Ir monometallic catalysts, as illustrated in Fig. 7. It can be seen that the amounts of NO desorbed from the Ir-based catalysts (Fig. 7A–D), especially, Ir–Au bimetallic samples, are higher than that from the Au-DD (Fig. 7E) or Al_2O_3 (Fig. 7F), indicating that the Ir-based catalysts have stronger ability for NO adsorption than Au metal catalyst or alumina support. Although the amount of NO desorption from Ir-CD and Ir–Au-CD are similar to the Ir-DD and Ir–Au-DD, respectively, it seems that the desorption profiles of other molecules are different between them. When we compare the peaks of $m/e = 44$, which correspond to the amount of N_2O formed, it is clear that the N_2O formation peaks over the dendrimer-derived samples are sharp and high at around 325 °C, whereas, over conventional-derived samples, they are relatively broader and smaller. Moreover, accompanying N_2O formation, N_2 was also formed on these catalysts (indicated by the peaks of $m/e = 28$). However, the observed N_2 formation peaks were much smaller than N_2O formation peaks over these samples. It is known that the N_2 as well as N_2O formation in this case is via the following paths [65]:

$$NO + * \rightarrow NO* \quad (2)$$

$$NO* \rightarrow N* + O* \quad (3)$$

$$N* + N* \rightarrow N_2 + 2* \quad (4)$$

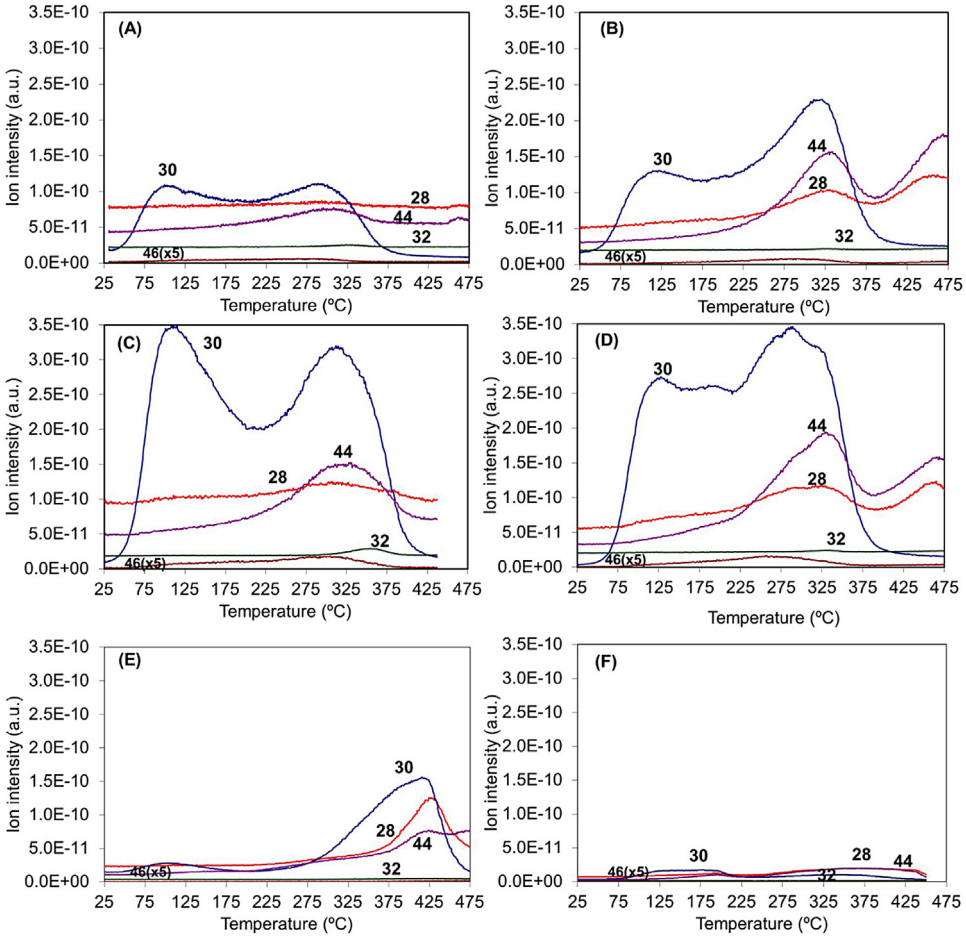

Fig. 7. NO-TPD over (A) Ir-CD, (B) Ir-DD, (C) Ir–Au-CD, (D) Ir–Au-DD, (E) Au-DD catalysts and (F) Al_2O_3 support; m/e: 30 NO, 32 O_2, 28 N_2, 44 N_2O and 46 NO_2.

Table 3
NO–CO reaction TOFs for all catalysts.

Catalysts	Surface site amount (atoms/g cat) × 10^{-18}	NO–CO TOFs (min^{-1}) at different temperature (°C)			
		25	100	200	250
Ir-CD	23.2 ± 2.2	0	3.9	8.7	38.6
Ir-DD	20.5 ± 2.7	0	22.1	33.2	57.2
Ir–Au-CD	3.1 ± 0.3	0	187.5	184.6	395.0
Ir–Au-DD	13.5 ± 1.1	0	33.0	41.5	69.9

$$N* + NO* \rightarrow N_2O + 2* \quad (5)$$

$$O* + O* \rightarrow O_2 + 2* \quad (6)$$

According to the above mechanism and NO-TPD results over the Ir–Au bimetallic catalysts, it can be concluded that NO dissociation on the surface of a catalyst is considered to be the key step.

It should be mentioned that, different from N_2 desorption, the desorption of O_2 (corresponding to $m/e = 32$) was not detected well in this case, probably because oxygen was more strongly bound on the catalyst surfaces than N_2. The same phenomena were also observed by Shi et al. [66].

3.5. Catalytic activity

In order to investigate the intrinsic activity of Ir and elucidate further the effect of Au on catalytic performance, the turnover frequencies (TOFs) were calculated as a function of different reaction temperature over the conventional and dendrimer-derived Ir–Au bimetallic catalysts and the Ir monometallic catalysts for both the NO–CO reaction (Fig. 8A) and direct NO decomposition (Fig. 8B), respectively. These TOFs were expressed as mole of NO reduced to N_2 and N_2O per mole of surface iridium atom and per minute, as listed in Tables 3 and 4. Since NO conversions were higher than 30% above 300 °C, only the reaction temperature up to 250 °C was considered for TOFs of NO–CO reaction, whereas the entire reaction temperature region up to 500 °C was considered for direct NO decomposition.

For the NO–CO reaction, it was interesting that the TOF gradually increased with decreasing iridium dispersion, irrespective of the catalysts, at the same reaction temperature. The Ir-CD sample with the highest iridium dispersion, $D_{Ir} = 74\%$, showed the lowest activity over the entire temperature range based on the calculated TOF values. The Ir-DD sample with iridium dispersion of 65% exhibits slightly better activity, followed by Ir–Au-DD ($D_{Ir} = 43\%$). Finally, the maximum TOF of NO–CO reaction was attained over Ir-Au-CD with iridium dispersion of 10%. By comparing Ir-DD and Ir–Au-DD, there was no great difference in TOF, as can be seen in Fig. 8A. This indicates that highly dispersed Au metal due to the dendrimer templating approach in this bimetallic sample does not affect the activity of the catalyst, although there is an electronic effect between Au and Ir observed in the sample based on the blue shift of IR peaks. In contrast, simply adding Au metal on Ir-Au-CD sample led to decrease Ir dispersion that is attributed to diluting surface Ir sites by Au and a concurrent change the intrinsic properties of the catalyst. Thus, with such a low dispersion, the TOF increased dramatically due to the possible geometric effect of more weakly bound CO or NO on smaller Ir ensembles with presence of Au, as we observed a red shift in the FTIR spectrum. However, it should be noted that the increased activity per surface atom at low dispersion is offset by the decrease in the number of surface atoms. However, these results clearly indicate that NO reduction

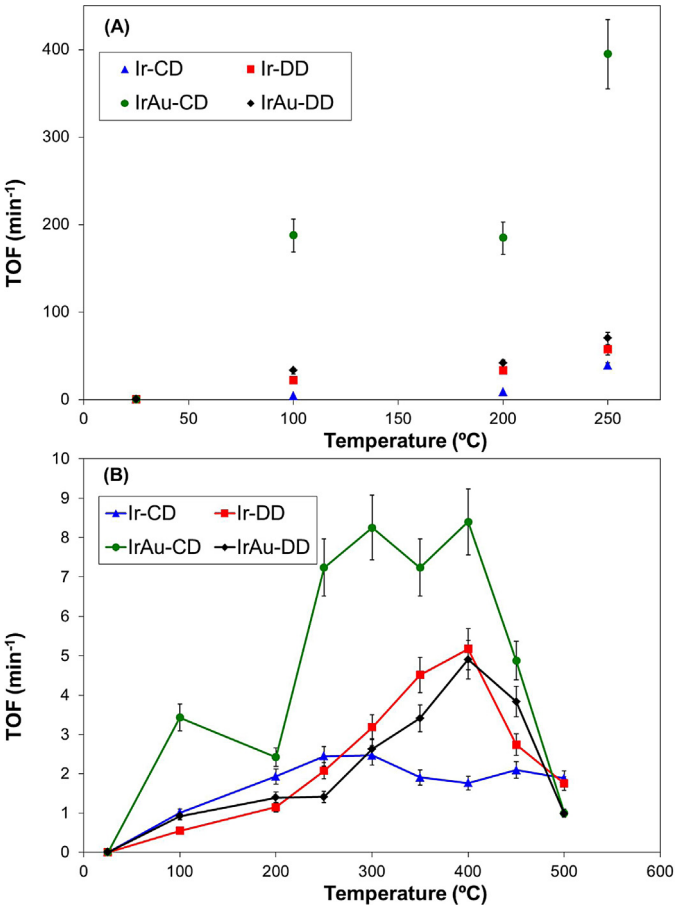

Fig. 8. . TOF of (A) NO–CO reaction (B) NO decomposition reaction over Ir monometallic and Ir–Au bimetallic catalysts.

Table 4
NO reaction TOFs for all catalysts.

Catalysts	Surface site amount (atoms/g cat) × 10^{-18}	NO TOFs (min^{-1}) at different temperature (°C)								
		25	100	200	250	300	350	400	450	500
Ir-CD	23.2 ± 2.2	0	1.0	1.9	2.4	2.5	1.9	1.8	2.1	1.9
Ir-DD	20.5 ± 2.7	0	0.5	1.1	2.1	3.2	4.5	5.2	2.7	1.8
Ir–Au-CD	3.1 ± 0.3	0	3.4	2.4	7.2	8.3	7.2	8.4	4.9	1.0
Ir–Au-DD	13.5 ± 1.1	0	0.9	1.4	1.4	2.6	3.4	4.9	3.8	1.0

with CO over Ir-based catalysts seems to be a structure-sensitive reaction.

Similar results were obtained for direct NO decomposition as shown in Fig. 8B. The Ir–Au-CD sample with the lowest iridium dispersion of 10% showed the highest activity over the entire temperature range based on the calculated TOF values. Such an enhanced TOF was presumably attributed to altered surface structure by Au that changes the intrinsic catalytic activities for NO–CO and NO reactions by varying the surface structure. However, it eventually diminished the Ir surface active sites that are available for such reactions and led to poor catalytic performance with lower NO conversion compared with activity on Ir monometallic catalysts as shown in Figs. 4 and 6. On the other hand, both dendrimer-derived Ir monometallic and Ir–Au bimetallic catalysts exhibited similar TOF values over an entire reaction temperature region, suggesting that Au metal does not play a significant role in those materials in this reaction. It should be noted that the TOF values for direct NO decomposition are much smaller (typically by at least an order of magnitude) than those for the NO–CO reaction on the same series of catalysts. This is attributed to the very strong adsorption of atomic oxygen on the surface of Ir and the lack of an appropriate reducing agent to remove these species. Thus, many of the active sites counted by chemisorption are likely poisoned by adsorbed atomic oxygen, as has been pointed out by others (e.g., [66,67]).

4. Conclusions

In this research, we prepared the Ir–Au bimetallic catalyst by using both dendrimer templating (Ir–Au-DD) and conventional incipient wetness (Ir–Au-CD) methods. The dendrimer-derived sample showed highly dispersed particles with very narrow particle size distribution confirmed by STEM and H_2 chemisorption measurements, compared to the conventionally-derived sample. As a result, the Ir–Au-DD sample exhibited better catalytic performance in NO reduction by CO and NO decomposition reaction compared with Ir–Au-CD sample. NO-TPD results also illustrate sharper and larger N_2O formation peaks for the dendrimer-derived sample. In addition, the effect of Au in Ir–Au bimetallic catalysts was investigated by calculating TOFs. From these results, it was noticed that catalytic properties for the reduction of NO by CO and direct decomposition of NO over the Ir–Au bimetallic catalysts appear to be structure sensitive. For the case of dendrimer-derived Ir–Au catalyst, there was no great difference in TOF by comparison to an Ir monometallic catalyst, suggesting that highly dispersed Au metal does not affect to the activity of the catalyst. In contrast, higher TOF was obtained for the Ir–Au-CD sample than for Ir-CD, and this was most likely due to a geometric effect involving a dilution of Ir surface sites by Au.

Acknowledgments

This work was financially supported by Toyota. The authors would like to acknowledge the University of South Carolina Electron Microscopy Center for instrument use, scientific and technical assistance, especially the assistance of Dr. Douglas A. Blom. We also thank Dr. Shuguo Ma with XPS facility and his support.

Appendix A. Supplementary data

Supplementary data associated with this article can be found, in the online version, at http://dx.doi.org/10.1016/j.apcatb.2014.01.065.

References

[1] A. Fritz, V. Pitchon, Appl. Catal., B 13 (1997) 1–25.
[2] H.S. Glick, J.J. Klein, W. Squire, J. Chem. Phys. 27 (1957) 850–857.
[3] J.W. Hightower, D.A.V. Leirsburg, in: R.L. Klimisch, J.G. Larson (Eds.), The catalytic chemistry of nitrogen oxides, Plenum Press, New York, NY, 1975, p. 63.
[4] F. Garin, Appl. Catal., A 222 (2001) 183–219.
[5] A. Gervasini, P. Carniti, V. Ragaini, Appl. Catal., B 22 (1999) 201–213.
[6] R. Burch, T.C. Watling, Catal. Lett. 37 (1996) 51–55.
[7] S.J. Tauster, L.L. Murrell, J. Catal. 41 (1976) 192–195.
[8] K.C. Taylor, J.C. Schlatter, J. Catal. 63 (1980) 53–71.
[9] P. Biloen, F.M. Dautzenberg, W.M.H. Sachtler, J. Catal. 50 (1977) 77–86.
[10] V. Ponec, G.C. Bond, Stud. Surf. Sci. Catal. 95 (1995) 1–5.
[11] M. Kuhn, J.A. Rodriguez, J. Catal. 154 (1995) 355–363.
[12] W.M.H. Sachtler, Appl. Surf. Sci. 19 (1984) 167–180.
[13] S.-L. Peng, L.-Y. Gan, R.-Y. Tian, Y.-J. Zhao, Comput. Theor. Chem. 977 (2011) 62–68.
[14] J.-A. Wang, G. Aguilar-Rios, R. Wang, Appl. Surf. Sci. 147 (1999) 44–51.
[15] T. Yoshinari, K. Sato, M. Haneda, Y. Kintaichi, H. Hamada, Catal. Commun. 2 (2001) 155–158.
[16] T. Yoshinari, K. Sato, M. Haneda, Y. Kintaichi, H. Hamada, Appl. Catal., B 41 (2003) 157–169.
[17] M. Nawdali, E. Iojoiu, P. Gelin, H. Praliaud, M. Primet, Appl. Catal., A 220 (2001) 129–139.
[18] M. Nawdali, H. Praliaud, M. Primet, Top. Catal. 16 (2001) 199–204.
[19] T. Nakatsuji, Appl. Catal., B 25 (2000) 163–179.
[20] C. Wogerbauer, M. Maciejewski, A. Baiker, U. Gobel, Top. Catal. 16 (2001) 181–186.
[21] E. Iojoiu, P. Gelin, H. Praliaud, M. Primet, Appl. Catal., A 263 (2004) 39–48.
[22] C. Wogerbauer, M. Maciejewski, A. Baiker, Appl. Catal., B 34 (2001) 11–27.
[23] C. Wogerbauer, M. Maciejewski, A. Baiker, U. Gobel, J. Catal. 201 (2001) 113–127.
[24] C. Wogerbauer, M. Maciejewski, A. Baiker, J. Catal. 205 (2002) 157–167.
[25] A.Q. Wang, L. Ma, Y. Cong, T. Zhang, D.B. Liang, Appl. Catal., B 40 (2003) 319–329.
[26] A.Q. Wang, D.B. Liang, C.H. Xu, X.Y. Sun, T. Zhang, Appl. Catal., B 32 (2001) 205–212.
[27] R.W.J. Scott, O.M. Wilson, S.K. Oh, E.A. Kenik, R.M. Crooks, J. Am. Chem. Soc. 126 (2004) 15583–15591.
[28] D.A. Tomalia, A.M. Naylor, W.A.I. Goddard, Angew. Chem. Int. Ed. 29 (1990) 138–175.
[29] J.M. Frechet, Science 263 (1994) 1710–1715.
[30] R.M. Crooks, B.I. Lemon, L. Sun, L.K. Yeung, M.Q. Zhao, Top. Curr. Chem. 212 (2001) 81–135.
[31] R.M. Crooks, M.Q. Zhao, L. Sun, V. Chechik, L.K. Yeung, Acc. Chem. Res. 34 (2001) 181–190.
[32] O.S. Alexeev, A. Siani, G. Lafaye, C.T. Williams, H.J. Ploehn, M.D. Amiridis, J. Phys. Chem. B 110 (2006) 24903–24914.
[33] D.S. Deutsch, A. Siani, P.T. Fanson, H. Hirata, S. Matsumoto, C.T. Williams, M.D. Amiridis, J. Phys. Chem. C 111 (2007) 4246–4255.
[34] D.S. Deutsch, C.T. Williams, M.D. Amiridis, in: J.R. Regalbuto (Ed.), Catalyst Preparation: Science and Engineering, CRC Press/Taylor & Francis, Boca Raton, FL, 2007.
[35] G. Lafaye, A. Siani, P. Marecot, M.D. Amiridis, C.T. Williams, J. Phys. Chem. B 110 (2006) 7725–7731.
[36] H. Xie, J.Y. Howe, V. Schwartz, J.R. Monnier, C.T. Williams, H.J. Ploehn, J. Catal. 259 (2008) 111–122.
[37] D.S. Deutsch, G. Lafaye, D.X. Liu, B. Chandler, C.T. Williams, M.D. Amiridis, Catal. Lett. 97 (2004) 139–143.
[38] H.F. Lang, R.A. May, B.L. Iversen, B.D. Chandler, J. Am. Chem. Soc. 125 (2003) 14832–14836.
[39] Y.-J. Song, Y.M. López-De Jesús, P.T. Fanson, C.T. Williams, J. Phys. Chem. C 117 (2013) 10999–11007.
[40] Y.M. López-De Jesús, A. Vicente, G. Lafaye, P. Marecot, C.T. Williams, J. Phys. Chem. C 112 (2008) 13837–13845.
[41] Y.M. López-De Jesús, C.T. Williams, Catal. Lett. 132 (2009) 430–437.
[42] H.G. Lang, S. Maldonado, K.J. Stevenson, B.D. Chandler, J. Am. Chem. Soc. 126 (2004) 12949–12956.
[43] M. Nemanashi, R. Meijboom, J. Colloid Interface Sci. 389 (2013) 260–267.
[44] G. Lafaye, C.T. Williams, M.D. Amiridis, Catal. Lett. 96 (2004) 43–47.
[45] J.R. Anderson, Structure of metallic catalysts, Academic Press, London; New York, 1975.
[46] D.S. Deutsch, PhD Dissertation. University of South Carolina, ProQuest, UMI Dissertations Publishing, 2006, 3245396.
[47] M. Haruta, Catal. Today 36 (1997) 153–166.
[48] Y. Iizuka, H. Fujiki, N. Yamauchi, T. Chijiiwa, S. Arai, S. Tsubota, M. Haruta, Catal. Today 36 (1997) 115–123.
[49] M. Haruta, M. Date, Appl. Catal., A 222 (2001) 427–437.
[50] F. Solymosi, J. Rasko, J. Catal. 62 (1980) 253–263.
[51] J.B. Lefers, P.J. Van den Berg, Anal. Chem. 52 (1980) 1424–1426.
[52] A. Bourane, M. Nawdali, D. Bianchi, J. Phys. Chem. B 106 (2002) 2665–2671.
[53] P. Gelin, G. Coudurier, Y. Bentaarit, C. Naccache, J. Catal. 70 (1981) 32–40.
[54] C.R. Guerra, J.H. Schulman, Surf. Sci. 7 (1967) 229–249.
[55] R.F. Howe, J. Catal. 50 (1977) 196–199.
[56] L. Lynds, Spectrochim. Acta 20 (1964) 1369–1372.
[57] F. Solymosi, E. Novak, A. Molnar, J. Phys. Chem. 94 (1990) 7250–7255.
[58] F.J.C.M. Toolenaar, A.G.T.M. Bastein, V. Ponec, J. Catal. 82 (1983) 35–44.
[59] T.I. Koranyi, J. Mihaly, E. Pfeifer, C. Nemeth, T. Yuzhakova, J. Mink, J. Phys. Chem. A 110 (2006) 1817–1823.

[60] A. Erdohelyi, K. Fodor, G. Suru, Appl. Catal., A 139 (1996) 131–147.
[61] A.A. Davydov, Infrared Spectroscopy of Adsorbed Species on the Surface of Transition Metal Oxides, Wiley, Chichester, New York, NY, 1990.
[62] R.J. Wu, T.Y. Chou, C.T. Yeh, Appl. Catal., B 6 (1995) 105–116.
[63] S. Qun, L. Landong, H. Zhengping, X. Zhi Ping, Appl. Catal., B 84 (2008) 734–741.
[64] J.H. Holles, R.J. Davis, T.M. Murray, J.M. Howe, J. Catal. 195 (2000) 193–206.
[65] H. Permana, K.Y. Simon Ng, C.H.F. Peden, S.J. Schmieg, D.K. Lambert, D.N. Belton, Catal. Lett. 47 (1997) 5–15.
[66] C. Shi, M. Cheng, Z. Qu, X. Yang, X. Bao, Appl. Catal., B 36 (2002) 173–182.
[67] F. Dhainaut, Y. Reneme, S. Pietrzik, Y. Schuurman, C. Mirodatos, P. Granger, Top. Catal. 56 (2013) 279–286.